



# Journal of Applied and Computational Mechanics



Research Paper

## Numerical Analysis on the Bond Performance of Different Anchored Joints under Monotonic and Cyclic Pull-push Loading

Rui Micaelo<sup>1</sup>, Marta Carvalho<sup>2</sup>, Raquel Almeida<sup>3</sup>, Wan-Yang Gao<sup>4</sup>, Hugo Biscaia<sup>5</sup>

<sup>1</sup> CERIS, CESUR and Department of Civil Engineering, NOVA School of Science and Technology, Portugal, Email: ruilm@fct.unl.pt

<sup>2</sup> UNIDEMI, Department of Mechanical and Industrial Engineering, NOVA School of Science and Technology, Largo da Torre, Caparica, 2825-149, Portugal, Email: mip.carvalho@fct.unl.pt

<sup>3</sup> UNIDEMI, Department of Mechanical and Industrial Engineering, NOVA School of Science and Technology, Largo da Torre, Caparica, 2825-149, Portugal, Email: raa@fct.unl.pt

<sup>4</sup> School of Naval Architecture, Ocean and Civil Engineering, Shanghai Jiao Tong University, 800 Dongchuan Road, Shanghai, 200240, China, Email: wanyanggao@sjtu.edu.cn

<sup>5</sup> UNIDEMI, Department of Mechanical and Industrial Engineering, NOVA School of Science and Technology, Largo da Torre, Caparica, 2825-149, Portugal, Email: hb@fct.unl.pt

Received September 24 2021; Revised November 23 2021; Accepted for publication November 27 2021.

Corresponding author: H. Biscaia (hb@fct.unl.pt)

© 2022 Published by Shahid Chamran University of Ahvaz

**Abstract.** This study aims to mitigate the gap of knowledge on the cyclic bond behaviour of Carbon Fiber Reinforced Polymer (CFRP) bonded onto a steel substrate. The Distinct Element Method was used to model different bonding techniques such as Externally Bonded Reinforcement (for reference purposes); the linear increase of the width of the CFRP composite; the assumption of a mixed adhesive; and using an additional steel plate bonded on the top of the CFRP. Compared with the monotonic loading simulations, the load capacity and ductility of the joints with the lowest overlapped bonded lengths decreased with the number of cycles. However, the strength of the CFRP-to-steel joints was not affected if the overlapping bonded joint had a long length.

**Keywords:** Bond; Cyclic loading; Damage; Numerical simulations; Distinct Element Method.

### 1. Introduction

Although the bonding technique has ancient usage, the diversity of its uses in many industries has never been as broad as it is now. The use of an adhesive to bond two lightweight materials without increasing the joint's final weight, or to create a joint that can eliminate stress concentration issues, are just a few of the reasons that justify the growth of the bonding technique in various industry sectors such as automotive, construction, aerospace, naval, and others. Several joining configurations may be found in the literature, e.g. [1-9]. Although the advantages of each configuration can be obvious when it comes to finding out which one can provide higher strength, complete comprehensive knowledge of their bond performance is a subject that is still far away to be achieved. Nonetheless, several authors have proposed analytical [10-13] or numerical [14-18] approaches to better understand the bond behaviour of a hybrid bonded joint when subjected to mechanical loading [19-24] and/or a temperature change [25-29]. However, when subjected to cyclic loading, the existing literature is still limited and, therefore, more research is needed to mitigate this gap.

Adhesively bonded structures have gained considerable relevancy in the industry because of their benefits over structures using mechanical steel fasteners. By following the bonding method, the final weight of the structures is decreased, and the stress concentrations can be eliminated. So, once the necessity for drilling holes is no longer needed to carry out, some money can be saved on manpower with subsequent impact on the final price of the structure. Moreover, by making holes in materials such as steel or aluminium, especially when Fibre Reinforced Polymers (FRP) are externally applied to the structure, the fatigue lifetime of the metallic structure can be reduced. Thereby, the bonding method can be a good alternative to the use of steel mechanical fasteners.

Different loading types should be addressed in the design of bonded joints since the integrity of these joints should be preserved over the lifetime of the structure. Despite the influence of the mechanical and/or thermal loadings has been extensively investigated, the long-term durability [30-34] and loading (i.e. creep) [35-37] behaviour of these joints have received far less attention. The cyclic or fatigue bond behaviour of joints has been largely disregarded so far, and the previous research accessible in the literature [38-44] are devoted to carbon (C)FRP composites externally bonded to concrete prisms.

The Cohesive Zone Modelling (CZM) was used to study and characterize the joining between FRP composites to a parent material. The CZM assumes that the contact between materials can be simulated by a non thickness material mechanically characterized through a bond stress vs. relative displacement (or slip) relationship. This CZM can be empirically calibrated, and the local bond-slip relationship can take different forms depending on the substrate [45], resin [46, 47], or applied external



compression stress conditions [48]. Due to the crack formation and development in concrete, a local nonlinear bond-slip relationship with exponential behaviour [22, 45, 30-32] can be associated with FRP-to-concrete bonded joints, whereas FRP-to-steel bonded joints are more likely to locally behave according to bi-linear or tri-linear bond-slip relationships [45-48]. Nonetheless, all the previously described local behaviours were derived from a monotonic loading test, and the bond behaviour of these joints when frequently loaded and reloaded remains almost unknown and further research is needed to enhance the actual understanding of this topic.

For instance, the local dissipated energy obtained from the bonded joints when subjected to cyclic loading is not well known and establishing a connection between the local and global dissipated energies of the joint during the debonding process would be interesting to obtain since it would allow us to better understand how the strength of the joint would degrade based on the local bond behaviour and vice versa [49]. Furthermore, such correlation would facilitate the development of computational strategies to predict the bond degradation of bonded joints subjected to cyclic loading, as well as to predict the strength evolution of the bonded joint as the number of loading cycles increases.

Some publications, e.g. [42-44], have already presented local bond-slip models capable of dealing with cyclic loading and allowing numerical analysis of the bond between a CFRP externally bonded to a concrete substrate. Martinelli and Caggiano [42], for example, provided a straightforward unified model for predicting the monotonic or cyclic bond behaviour of FRP-to-concrete interfaces. The crack opening is compatible with fracture mode II, and their model [42] is based on a standard second-order differential equation commonly utilized by numerous authors, e.g. [27, 50-53]. In this case, the local bond-slip relationship under monotonic loading is also assumed to be known *a priori*. The softening stage of this bond-slip relationship is assumed to have an exponential or linear configuration. The model implies that the deterioration of interfacial stiffness during the unloading phase is proportional to the value of the dissipated energy at each location of the interface. When compared to the experimental load-slip results obtained by Ko and Sato [38], the Martinelli and Caggiano's model [42] indicated that the numerical results were quite accurate with the experimental ones, but the values of the residual slips were underestimated. Furthermore, based on the comparisons made by the authors [42], they concluded that when the exponential softening branch was used instead of the linear one, which is generally accepted for the simulation of FRP-to-concrete bonded joints under monotonic loading, the numerical results were even more accurate with the experiments.

Carrara and De Lorenzis [43] presented a thermodynamically consistent model to predict the cyclic bond behaviour of FRP composites externally bonded to concrete. In addition to the typical parameters used to calibrate the local bond-slip relationship under monotonic response, this model [43] requires only one more parameter with a physical meaning to describe the mode II debonding between an FRP composite and a concrete substrate under cyclic loading. It is based also on a non thickness interface with plasticity, and during the unloading path, no bond stresses can be developed. Under monotonic loading, the model reproduces a bi-linear bond-slip relationship. The validation of the model was proved by comparing it to other experimental data from the literature where various cyclic loadings were considered such as, with variable amplitude cycles [38], with constant amplitude cycles [40], and with cyclic loading and post-fatigue behaviour [41]. The agreement between the numerical simulations and the experimental results was notable, but like the model proposed by Martinelli and Caggiano [42], the residual slips at the unloading stages of the experiments were underestimated [43]. Nonetheless, under cyclic loading conditions, the model proposed by Carrara and De Lorenzis [43] followed a small decrease of the ultimate slip (i.e., the slip beyond which no more bond stress transfer occurs between materials) which was experimentally observed as well.

Zhou et al. [44] also suggested a thermodynamically consistent damage plasticity model in which the damage parameter ( $D$ ) was determined by a polynomial function based on the ratio between the dissipated energy ( $w_d$ ) and the total interfacial fracture energy ( $G_f$ ). Like in the case of CFRP-to-concrete bonded joints [43], this damage function was found to also describe the damage progress of CFRP-to-steel bonded joints under cyclic loading. A local bi-linear bond-slip relationship is established under a monotonic loading condition and the model proposed by Zhou et al. [44] may assume negative bond stresses during the unloading paths. When confronted against other models available in the literature [42, 43], the load-slip responses of the bonded joints were comparable to the load-slip results of the bonded joints obtained from the model proposed by Martinelli and Caggiano [42]. It is noteworthy to mention also that only the model proposed by Carrara and De Lorenzis [43] can assume hysteresis loops, which explains the load decrease transmitted to the CFRP composite during the reloading paths.

As shown so far, the debate over the effect of the cyclic loading on adhesively bonded structures is currently ongoing, with researchers gathering data from laboratory experiments [38, 40, 41, 49] and developing numerical techniques [42-44] to improve their actual knowledge on this topic. Since no consensus numerical solutions have yet been found, and various local adhesive behaviours might be associated with different types of joints [46, 47, 54-56], more research on this topic is further needed. As a result, the current work attempts to mitigate the gaps in our understanding of the influence of cyclic loadings on CFRP-to-steel bonded joints by analysing a series of different bonding situations using the Distinct Element Method (DEM). The interface is modelled by a local bi-linear bond-slip relationship and a total of five different bonding techniques contemplating 40 different models were defined. The first set of specimens refers to the specimens where the Externally Bonded Reinforcement (EBR) was simulated, and the results were used as a reference which allowed us to evaluate the efficiency of each alternative bonding technique. Furthermore, monotonic and cyclic loading were examined, allowing us to investigate the effects of the cyclic bond behaviour on the specimens by comparing their results to their homologous specimens, i.e. the specimens with the same total bonded length subjected to monotonic loading.

The numerical results presented in this work are crucial not only to improve the actual knowledge on the cyclic bond behaviour of distinct bonding techniques but also it allows us to identify which is the most promising one and, therefore, worthy to be experimentally tested soon. The identification of the benefits and flaws associated with each bonding technique is carried out through the examination of the global load-slip response, the evolution of the debonded length of the joints, the local and global damage, the strength degradation of the CFRP-to-steel joints, and the equivalent damping factor.

## 2. Modelled Adhesively Bonded Joints and Test Protocols

### 2.1 Description of the adhesively bonded joints and anchorage systems

To investigate the bond performance of the five different bonding techniques subjected to the monotonic and cyclic loadings, a CFRP strip is adhesively bonded to a steel plate which compared with the CFRP strip can be assumed as a rigid substrate. The adhesively bonded CFRP-to-steel joint without an additional anchorage is known as Externally Bonded Reinforcement (EBR), and it was considered and modelled for comparison purposes and playing, therefore, the reference role in this work. The following three main anchorage techniques were studied: (i) with an additional bonded length where the width is linearly increased (VW); (ii) with an additional bonded length where two CZM are assumed which intend to simulate, e.g., the use of two distinct adhesives (MA); and (iii) with a steel plate bonded on top of the CFRP strip (SP). The five CFRP-to-steel bonded joints are subjected to a pull-push loading scheme which induces a debonding failure mode consistent with fracture mode II. Fig. 1 shows all the



simulated bonded joints and anchorage systems considered in this work. To each case, the top and side views of the bonded joint are presented as well as the representation of the numerical strategy based on the DEM which is further described in detail in Section 3. For the anchored joints, the total bonded length ( $L_t$ ) comprises the regular bonded length ( $L_b$ ), where EBR technique is adopted, and the anchorage length ( $L_a$ ).

The geometry of the simulated specimens consists of a CFRP laminate with a width ( $b_f$ ) of 10 mm and a thickness ( $t_f$ ) of 1.4 mm bonded to a rigid substrate, such as a thick steel plate. In this situation, the laminate to steel axial stiffness ratio is close to zero, and therefore the substrate of the joint can be modelled as a rigid body [57]. The properties of the CFRP laminate were adopted based on a series of previous experiments carried out by the authors [45] where several CFRP flat coupons were tested under a monotonic tensile load test until rupture. The average values of the elastic modulus ( $E_{fm}$ ) and the failure stress ( $\sigma_{f,um}$ ) and ultimate strain ( $\epsilon_{f,um}$ ) were, respectively, 159 GPa, 1565 MPa, and 1.03%. For the interfacial bond behaviour of the CFRP to the rigid substrate was admitted a bi-linear bond-slip model (denoted as CZM 1 in Fig. 2), with maximum bond stress ( $\tau_{max}$ ) of 13.27 MPa at an interfacial slip ( $U^s_{max}$ ) of 0.096 mm and an ultimate slip ( $U^s_{ult}$ ) of 0.256 mm beyond which the bond stresses are zero.

The VW type anchorage has been preliminary studied by the authors for concrete substrates [58], showing an improvement of the maximum load transmitted to the CFRP composite with a larger deformation under monotonic loading than the conventional EBR system. This can be explained by the increase of the CFRP width that directly increases the final strength of adhesively bonded joints [58]. In this study, the width of the bonded joint was increased three times over the anchorage length (see Fig. 1b), i.e.  $b_{vw} = 3b_f$ .

The MA type anchorage is built with a different adhesive from that used in the regular bonded area, i.e. on the CFRP pulled side of the bonded joint, and it should have the ability to increase the interfacial maximum bond stress and/or to increase the deformation of the joint through the increase of the ultimate interfacial slip. Within this perspective, two adhesives were idealized for the anchorage region. To locally define the bond-slip relationships that both adhesives would originate, the first one would be characterized by a maximum interfacial bond stress value of 19.90 MPa (corresponding to an increase of 50% from the original value of 13.27 MPa) with an interfacial slip of 0.144 mm (which is also 50% higher than its original value of 0.096 mm). This CZM model was defined as CZM 2 in Fig. 2c. On the other hand, the CZM 3 shown in Fig. 2c was idealized to sustain a greater interfacial slip at failure (0.384 mm) but preserving the same maximum interfacial bond stress and slip of CZM 2. Therefore, the elastic bond stiffness of the three CZM was kept unchanged.

The SP type anchorage increases the strength of the joint due to the bonded area that is increased by the additional bond surface between the CFRP composite and the steel plate. This means that the CFRP composite will stay bonded to a rigid substrate over the bottom and top surfaces. It is worthy to mention also that although it is possible to increase the strength of the anchorage by applying a compressive force on the (top) steel plate as documented in the literature [48, 55], such an option was not considered since depending on the external pressure imposed to the steel plate, the local bond behaviour would change also. Consequently, to take into account this effect, the CZM would be defined through a different bond-slip relationship, i.e. through a tri-linear bond-slip relationship with residual interfacial bond stress after the softening stage rather than a bi-linear bond-slip relationship [48, 55].

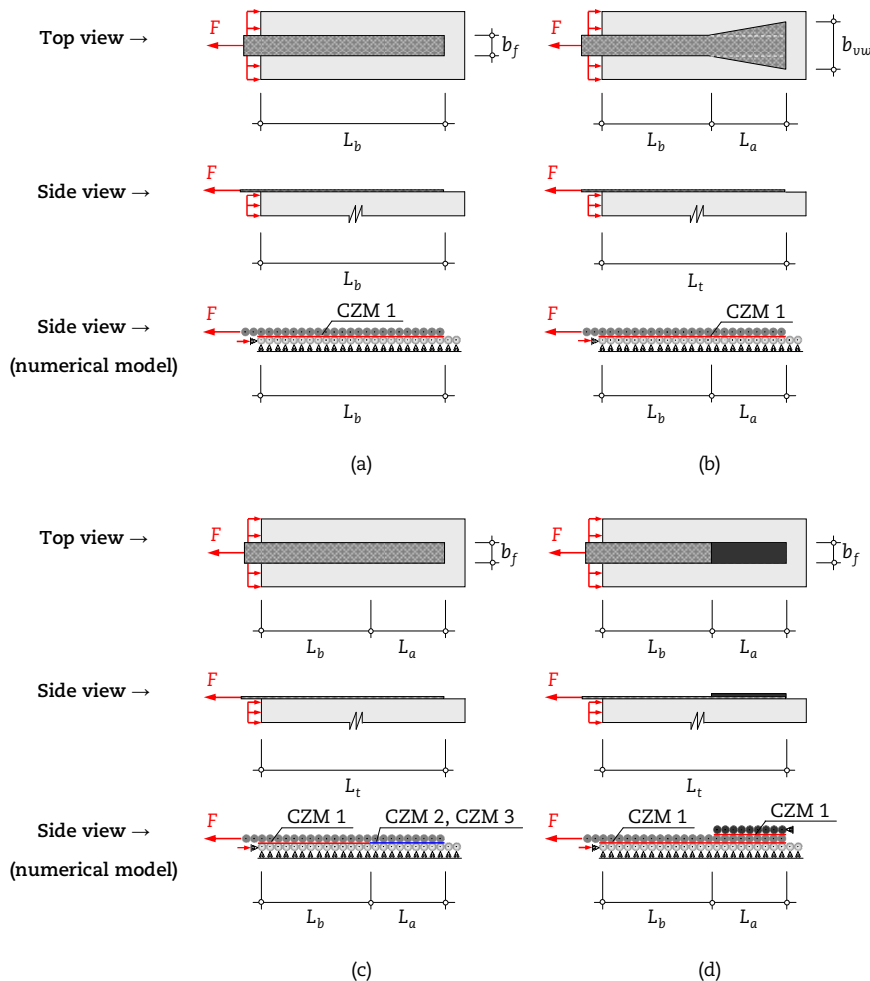


Fig. 1. Modelled adhesively bonded joints: (a) EBR; (b) EBR+VW; (c) EBR+MA-1 or EBR+MA-2; (d) EBR+SP.



Table 1. Modelled adhesively bonded joints.

Bonded joint	Test protocol	Total bonded length	Regular bonded length	Anchorage length
		$L_t$ (mm)	$L_b$ (mm)	$L_a$ (mm)
EBR		100	100	-
		200	200	-
		300	300	-
		400	400	-
EBR + VW		100	50	50
		300	250	50
		200	50	150
		400	250	150
BR + MA-1	Monotonic and Cyclic	100	50	50
		300	250	50
		200	50	150
		400	250	150
EBR + MA-2		100	50	50
		300	250	50
		200	50	150
		400	250	150
EBR + SP		100	50	50
		300	250	50
		200	50	150
		400	250	150

In addition, and since the bonded length is one of the most important factors for the mechanical performance of any bonded joint, different bonded lengths were considered in the two regions of the bonded interface (regular and anchorage). The adopted regular bonded lengths had 50 mm and 250 mm and their purpose was to study the situations where the bonded length is shorter and longer than the length required to reach the maximum strength of the joint, which is usually referred to as the effective bonded length ( $L_{eff}$ ). Like the regular bonded lengths, two different anchorage lengths were considered in this work, one with only 50 mm whilst the other had 150 mm. Hence, four lengths combinations were simulated for each anchorage type. To compare the results between the conventional joint system (EBR) and the CFRP bonded joints with different anchorages the same total lengths were simulated with the EBR. Table 1 lists the twenty CFRP-to-steel bonded joints modelled in this study under the monotonic and cyclic loading. To facilitate the identification of each specimen, the bonded joints are referred to in the text by type and total length, e.g. "EBR+VW-200" corresponds to the bonded joint with EBR followed by a variable-width region (anchorage) and a total bonded length of 200 mm.

## 2.2 Loading protocols

As already mentioned, the mechanical behaviour of the adhesively bonded joints was evaluated under a numerically simulated pull-push single-lap shear test. The simulations were carried out in a displacement control mode whether when subjected to monotonic or cyclic loading. As it was illustrated in Fig. 1, the left side of the CFRP strip is pulled while the steel substrate displacements are constrained in the pulled direction. The anchorage is in the far-end right of the CFRP-to-steel bonded joint, i.e. localized at the opposite to the CFRP pulled end. By adopting the displacement control mode, the interfacial slip at the pulled end between the bonded elements is the same for all the CFRP-to-steel bonded joints at a defined simulation point.

In the monotonic loading, the CFRP strip was pulled out at constant displacement speed until failure, which can occur at the CFRP (if the tensile strength is reached) or within the interface (cohesive failure mode within the adhesive). As will be seen later, all simulated CFRP-to-steel bonded joints had a typical cohesive failure within the adhesive. For the simulation of the loads transmitted to the CFRP strip, a displacement speed of 10 mm/s was applied to the CFRP pulled end whether when subjected to the monotonic or to the cyclic loading.

The simulated cyclic loading protocol consisted in applying consecutive loading cycles where the maximum interfacial slip was increased periodically. Based on the bond-slip relationships previously described, ten maximum interfacial slip values were considered: 0.136 mm; 0.176 mm; 0.216 mm; 0.256 mm; 0.296 mm; 0.376 mm; 0.536 mm; 0.856 mm; 1.496 mm; and 2.776 mm. These interfacial slip amplitudes were increased at every three loading cycles. The end of all unloading paths was suspended when the registered load was equal to or lower than 250 N preventing, therefore, that the CFRP strip could be pushed during the cyclic loading protocol. Table 2 resumes this loading protocol.

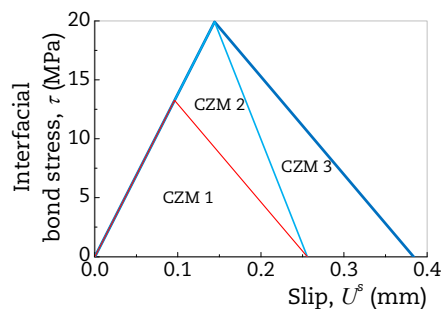


Fig. 2. Interfacial bond-slip models adopted.



**Table 2.** Cyclic loading protocol conditions.

Cycle	Loading phase	Unloading phase
	Maximum $U^s$ (mm)	Minimum $F$ (N)
1, 2, 3	0.136	250
4, 5, 6	0.176	
7, 8, 9	0.216	
10, 11, 12	0.256	
13, 14, 15	0.296	
16, 17, 18	0.376	
19, 20, 21	0.536	
21, 22, 23	0.856	
24, 25, 26	1.496	
27, 28, 29	2.776	
30	Until failure	Not applicable

### 3. Numerical Strategy using the Distinct Element Method

#### 3.1 Description of the method

The numerical models follow the general concepts of the Distinct Element Method (DEM) firstly introduced by Cundall in the 1970s for the study of rock fracture problems, and since then adapted for the study of different problems [59]. The materials are represented by an assembly of rigid particles which interact with each other through soft contact points, and the displacement and rotation of each particle are related to the set of forces acting on it. The calculations consist of the repeated application of the law of motion, based on Newton’s second law, to each particle, followed by the force-displacement law at the contact points. Different contact models, with and without bonding, can be adopted with this soft contact approach, which means that rigid particles can overlap each other at contacts when in compression. During the numerical process, existing contacts can be broken, and new contacts can be created from the update of the particle’s relative position. Two and three-dimensional formulations have been developed, such as described in [60, 61]. This methodology is conceptually simple, however, the computational effort is usually higher than with continuum-based formulations, and increases with the number of particles in the assembly and the reduction of the time step between calculation cycles.

A two-dimensional (2D) collection of circular rigid-particles (cylinders), equally-sized, were used in this study to model the CFRP and the substrate. The cylinders are vertically aligned on a single plane, meaning that two force components and one moment component act at the particle’s centroid, and the out-of-plane force component and two moment components are not considered in the calculation cycle. The assembly of particles and the displacement’s restrictions imposed on each bonded joint and anchorage system modelled is shown in Fig. 1. This methodology was used before with success to analyse the performance of CFRP-to-concrete [58, 62] and CFRP-to-steel bonded joints [63], showing the ability to represent their mechanical behaviour under different conditions of applied loading and interfacial bond-slip relationships.

#### 3.2 Contact constitutive models

From the previous description of the adopted materials to be used in the simulation of the CFRP-to-steel bonded joints, two different contact laws were used to model the interaction between particles representing the CFRP and the interface between adherends. The substrate was considered rigid, and the force-displacement law was not applied to the contacts between the substrate’s particles. For the CFRP the force-displacement law is linear elastic with fragile rupture under tension, as illustrated in Fig. 3a, where  $k_e^n$  is the elastic slope and  $U^{n,ult}$  is the displacement at failure.

The CFRP to rigid substrate (shear) bond was modelled with a bi-linear bond-slip relationship with an unloading-reloading path parallel to the linear elastic branch (see Fig. 3b). Upon monotonic loading, the elastic branch stiffness is  $k_e^s$ , and the softening branch stiffness  $k_d^s$  initiates at  $\tau_{max}$ . The slip at  $\tau_{max}$  is  $U_{max}^s$ , and at failure ( $\tau = 0$ ) is  $U_{ult}^s$ . Upon cyclic loading, with repeated unloading and reloading, the unloading-reloading stiffness is kept constant ( $k_e^s$ ) but the stress threshold value ( $\tau_{max,n}$ ) decreases with the accumulated plastic displacement ( $U_{p,n}^s$ ) of the interface at cycle  $n$  according to the following equation:

$$\tau_{max}(U_{p,n}^s) = \pm \tau_{max} \cdot \left( 1 - \frac{U_{p,n}^s}{U_{ult}^s - U_{max}^s} \right). \tag{1}$$

Plastic displacement accumulates when the maximum shear stress exceeds the stress threshold value provided from Eq. (1). The maximum accumulated plastic displacement, corresponding to bond failure, is the amplitude of the softening branch of the bi-linear bond-slip relationship, i.e.  $U_{ult}^s - U_{max}^s$ .

So, for cycle  $n$ , at the end of the (re)loading path (simulation point  $n - 0.5$ ) with the interfacial slip  $U_n^s$ , the contact bond stress of the interface is defined according to:

$$\tau(U^s) = \begin{cases} k_e^s U_n^s & \text{if } U_{p,n}^s = 0 \\ \tau_{n-0.5} + k_e^s \cdot (U_n^s - U_{n-0.5}^s) & \text{if } U_{p,n}^s = U_{p,n-0.5}^s \\ \tau_{max,n} - \tau_{max} \cdot \left( \frac{U_{p,n}^s - U_{p,n-0.5}^s}{U_{ult}^s - U_{max}^s} \right) & \text{if } U_{p,n-0.5}^s < U_{p,n}^s < U_{ult}^s - U_{max}^s \end{cases} \tag{2}$$

and the accumulated plastic displacement is

$$U_p^s = U_{p,n-0.5}^s + \begin{cases} 0 & \text{if } U_n^s < U_{n-0.5}^s + \frac{\tau_{max,n} - \tau_{n-0.5}}{k_e^s} \\ U_n^s - \left( U_{n-0.5}^s + \frac{\tau_{max,n} - \tau_{n-0.5}}{k_e^s} \right) & \text{if } U_n^s > U_{n-0.5}^s + \frac{\tau_{max,n} - \tau_{n-0.5}}{k_e^s} \end{cases} \tag{3}$$



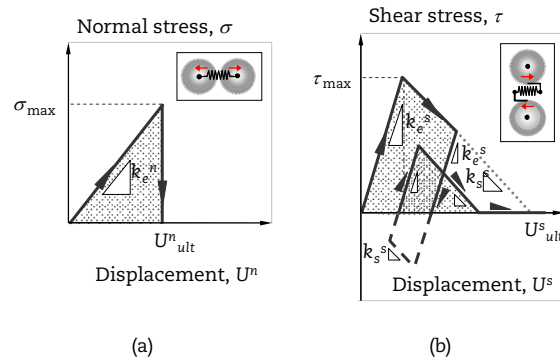


Fig. 3. Contact laws adopted in the simulation: (a) CFRP to CFRP contacts; and (b) CFRP to substrate (shear) bond-slip model.

while, in the end of the unloading path (simulation point  $n$ ) the contact bond stress is

$$\tau(U^s) = \begin{cases} k_e^s U_n^s & \text{if } U_{p,n}^s = 0 \\ \tau_{n-0.5} - k_e^s \cdot (U_{n-0.5}^s - U_n^s) & \text{if } U_{p,n}^s = U_{p,n-0.5}^s \\ \tau_{\max,n} + \tau_{\max} \cdot \left( \frac{U_{p,n}^s - U_{p,n-0.5}^s}{U_{\text{ult}}^s - U_{\max}^s} \right) & \text{if } U_{p,n-0.5}^s < U_{p,n}^s < U_{\text{ult}}^s - U_{\max}^s \end{cases} \quad (4)$$

and the accumulated plastic displacement is

$$U_p^s = U_{p,n-0.5}^s + \begin{cases} 0 & \text{if } U_n^s \geq U_{n-0.5}^s + \frac{\tau_{\max,n} - \tau_{n-0.5}}{k_e^s} \\ -U_n^s + \left( U_{n-0.5}^s + \frac{\tau_{\max,n} - \tau_{n-0.5}}{k_e^s} \right) & \text{if } U_n^s < U_{n-0.5}^s + \frac{\tau_{\max,n} - \tau_{n-0.5}}{k_e^s} \end{cases} \quad (5)$$

### 3.3 Interfacial (local) damage vs. global damage

The interfacial damage state of the CFRP-to-steel bonded joints can be described either from a global or local perspective. Thus, the global damage condition of the interface is determined from the length of the CFRP that has physically debonded from the substrate. To analyse this global parameter, the following normalized debonded length was defined as:

$$L_{d,n}^* = \frac{L_{d,n}}{L_t} \quad (6)$$

where  $L_{d,n}$  and  $L_t$  are the debonded length in cycle  $n$  and the total bonded length of each analysed specimen.

In addition, the interfacial damage can be described at every point of contact along the bonded length based on the local bond-slip relationship. The interfacial damage progression is proportional to the accumulated plastic displacement [63]. This means that when the (re)loading-unloading paths are within the elastic branch, there is no damage progression while the full damage state is obtained when the plastic displacement reaches its maximum value. From this, the local damage condition of every single point of the CFFP-to-steel joint varies between 0 (i.e. with no damage) and 1 (i.e. fully damaged), and at cycle  $n$  ( $D_n^U$ ) is calculated according to:

$$D_n^U = \frac{U_{p,n}^s}{U_{\text{ult}}^s - U_{\max}^s} \quad (7)$$

## 4. Results and Discussion

The numerical results of the adhesively bonded joints between the CFRP laminates and a steel substrate with different anchorage systems subjected to monotonic and cyclic loading under pull-push single-lap test scheme are presented and discussed in this section. To allow the understanding of the effects of the cyclic loading on the bond performance of different anchorage joints, the results, in terms of the global mechanical response with the load-slip evolution, obtained under monotonic loading are first described, and only then, the results obtained under cyclic loading are described and discussed in detail. The shear stress and strain distributions throughout the bonded length are analysed, and the local damage distribution obtained from Eq. (6), as well as the global damage evolution obtained from Eq. (7), are presented and discussed thoroughly.

### 4.1 Load-slip response of the specimens subjected to monotonic loading

Figure 4 compares the load-slip curves of the CFRP-to-steel bonded joints with the same total bonded length. Therefore, Fig. 4a and Fig. 4c show the load-slip curves of the specimens where the adopted anchorage length is 50 mm whereas Fig. 4b and Fig. 4d show the load-slip curves of the specimens with a mechanical anchorage with a length of 150 mm. All specimens have failed through the interface, i.e. the CFRP debonded from the steel substrate. The corresponding rupture load of the CFRP laminate is 22.9 kN which is a value that was never reached in the numerical simulations.



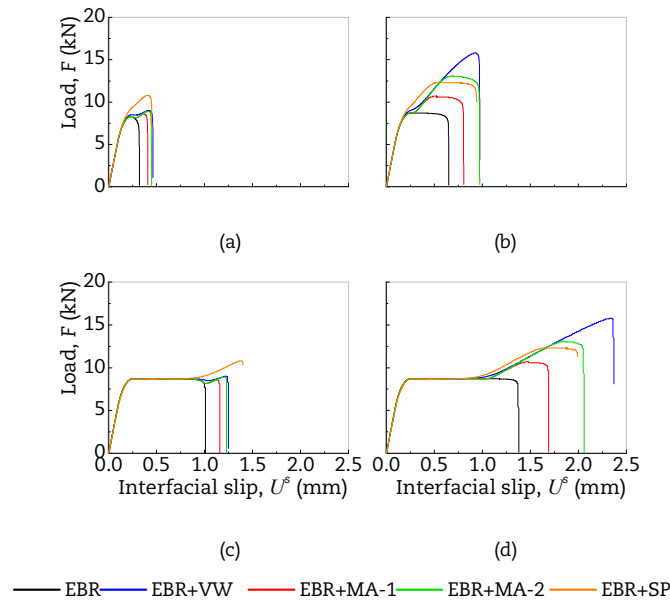


Fig. 4. Load-slip of numerical specimens with a total bonded length of: (a) 100 mm; (b) 200 mm; (c) 300 mm; and (d) 400 mm.

As initially expected, the effect of the bonded length on the load-slip curves is very relevant. For all tested specimens, as the total bonded length increases the interfacial slip at failure also increases. In the EBR specimens, the increase in the interfacial slip at failure was about 357% when the total bonded length has increased from 100 mm to 400 mm. This means that the ductility of the CFRP-to-steel bonded joint increases with the increase of the bonded length.

However, and except for the EBR specimens, the maximum load reached in all the mechanically anchored specimens increased substantially with the anchorage length. For the EBR type bonded joint, the maximum load was 8.27 kN, 8.69 kN, 8.70 kN, and 8.70 kN for, respectively, a total bonded length of 100 mm, 200 mm, 300 mm, and 400 mm. This reveals that the maximum load transmitted to the CFRP strip increases until a certain bonded length value is usually denoted as the effective bond length and from thereafter the increase of the bonded length does not affect the strength of the bonded joint. Hence, the effective bond length of the EBR specimens, i.e. corresponding to the reference situation where the CZM 1 is used, is between 100 mm and 200 mm.

Also, as initially assumed in this study, the anchored specimens are divided into two different groups, one corresponding to the specimens with a short anchorage length (50 mm) and the other one to a long anchorage length (150 mm). This allows us to evaluate the benefits of using different mechanical anchorage types with short and long anchorage lengths. The beneficial effect of the anchoring system on the strength of the CFRP-to-steel bonded joints is almost negligible when the anchorage length is small. However, for the EBR+SP specimens with only 50 mm of anchorage length, the strength of the bonded joint could be increased by almost 24-30%. Also, this effect does not change much when the regular bonded length of the specimens is longer than the effective length.

On the contrary, when the anchorage length is large, i.e. with 150 mm long, the beneficial effect can be very significant, and the results vary depending on the anchorage system used to anchor the CFRP laminate to the steel substrate. Thus, the strength increases in the EBR+VW, EBR+MA-1, EBR+MA-2, and EBR+SP specimens reached, respectively, 81%, 22%, 49%, and 41% of the reference values obtained from the EBR specimens. Nevertheless, even for EBR+VW which have reached the highest loads transmitted to the CFRP laminate was insufficient to ensure that the failure mode of the bonded joint could shift from cohesive within the adhesive (interface rupture) to cohesive in the CFRP laminate, i.e. by reaching the rupture load of the CFRP laminate.

In terms of the ultimate slip, all the CFRP-to-steel bonded joints increased the ductility of the joint. The range of this increase was 23-72% for the EBR+VW specimens, 15-33%, and 22-50% for the EBR+MA-1 and EBR+MA-2, respectively, and 40-47% for EBR+SP specimens. The least effect was always found for the CFRP-to-steel bonded joints with a total bonded length of 300 mm, i.e. with a regular bonded length of 250 mm with an anchorage length of 50 mm.

## 4.2 Mechanically anchored joints subjected to cyclic loading

### 4.2.1 Load-slip response

To assess the effect of the cyclic loading on the different CFRP-to-steel bonded joints, Fig. 5 makes the comparison between the load-slip curves obtained under monotonic and cyclic loading for each joint. Upon successive cycles with increasing maximum interfacial slips at the CFRP pulled end, the load is, in general, close to the load obtained from the monotonic loading situation. Also, the ultimate interfacial slips obtained in the specimens at the failure of the joints were almost identical whether the loading applied to them have a monotonic or a cyclic trend. The specimens with the longest total bonded length were able also to withstand a higher number of loading cycles before failure. For instance, the cycle corresponding to the failure of the specimens varied between the 16<sup>th</sup> (in the case of the EBR specimen with a bonded length of 50 mm) and the 28<sup>th</sup> (in the anchorage joints with  $L_t = 400$  mm) loading cycle.

On the contrary, it is observed from the results in Fig. 5 that the global stiffness of the bonded joints is significantly affected by the cumulative loading cycles imposed on the CFRP-to-steel bonded joints. This means that once the bonded joint has been already subjected to mechanical loading, new reloading of the joint until that previous load magnitude will be achieved at a higher interfacial slip. This bond behaviour is a consequence of the accumulated damage along the interface developed during the cyclic loading that the joint was previously subjected to.



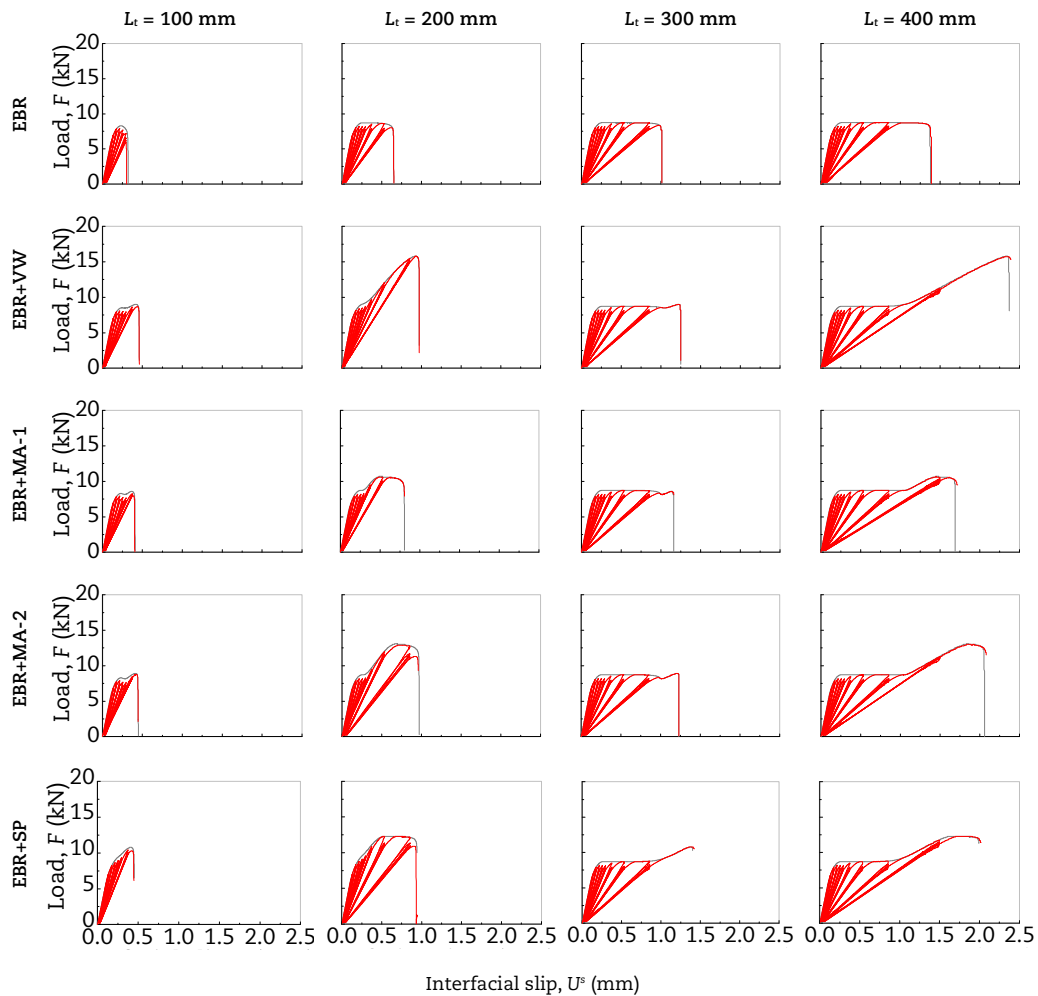


Fig. 5. Load-slip of all numerical specimens subjected to monotonic and cyclic test protocols.

In addition, Fig. 6 shows the evolution of the ratio between the maximum loads obtained from the cyclic loading ( $F_{\max,n}$ ) and the monotonic ( $F_{\max,m}$ ) at the same interfacial slip for the number of loading cycles. The total bonded length is constant in each graph plotted in Fig. 6. All curves obtained from the CFRP-to-steel joints exhibit a saw-tooth pattern with the loading cycles which is correlated to the applied loading protocol and the proposed cyclic bond-slip relationship (see Fig. 3b). In the simulated loading protocol, the amplitude of the interfacial slip was increased every three consecutive cycles (see Table 2), and due to the accumulated damage in the first of three cycles at the same slip amplitude, the load reached in the following cycles tend to decrease. Moreover, the load transmitted to the CFRP strip decreased with the increase of the slip amplitudes between the 2<sup>nd</sup> and the 4<sup>th</sup> amplitude step (i.e. corresponding to the 4<sup>th</sup> and 15<sup>th</sup> loading cycle, respectively), and then, it increased up to the point of the results obtained from the specimens under the monotonic loading condition in joints with a total bonded length of 200 mm, 300 mm and 400 mm. This can be attributed to the local bond-slip relationship as the 4<sup>th</sup> nominated slip amplitude was the ultimate slip considered in CZM 1 (see Fig. 2). In other words, after the interface has initiated its debonding process at the pulled end, the interfacial bond stresses move towards the CFRP unpulled end. Hence, considering the equilibrium conditions of the CFRP strip, if the bonded length is sufficiently long to fully install the bond stress diagram, then the maximum load reached in the specimens under the monotonic load condition can be attained once again. Under these circumstances, the strength of the CFRP-to-steel bonded joint will remain unchanged with the loading cycles.

#### 4.2.2 Shear stress and CFRP strain distribution throughout the bonded length

This subsection analyses the effect of the cyclic loading on the shear (or bond) stress and strain distribution along the bonded length. Figures 7 and 8 show, respectively, the shear stress and the CFRP strain distributions. The results herein presented are based on the target loading points in cycles 1 (interfacial slip of 0.136 mm), 7 (0.216 mm), 13 (0.296 mm), 19 (0.536 mm), 22 (0.856 mm) and 25 (1.456 mm). The results obtained from the cyclic loading event are compared with the results obtained from the monotonic loading at the same nominated interfacial slips or loading cycles. These cyclic loading points correspond to the first of three cycles that the defined interfacial slip at the CFRP pulled end is reached. It should be noted that the number of plotted curves depends on the maximum slip value reached at the CFRP pulled end in each bonded joint.

The interfacial stresses and CFRP strains variation with bonded length are very similar upon cyclic and monotonic loading. Thus, these results could be expected because of the similarity in global load-slip curves obtained with different loading protocols. The interfacial stresses curves vary significantly in the EBR and anchorage zones, and among different anchorage types. Each anchorage has specific bond characteristics that affect the stress variation with bonded length. However, in most situations, this does not mean a discontinuity of stress values at the point of separation between EBR and anchorage regions. This occurred because the three bond-slip models used (see Fig. 2) had the same elastic stiffness, and for most curves, the anchorage zone interface is in the elastic zone of the bond-slip model. As expected, when the anchorage region is long (150 mm in this study), the latter stress curves are fully installed within this region. This allows getting the most from the anchorage and justifies the low impact of short anchorages in increasing the load capacity and the ductility of the bonded joint in comparison with the conventional system.





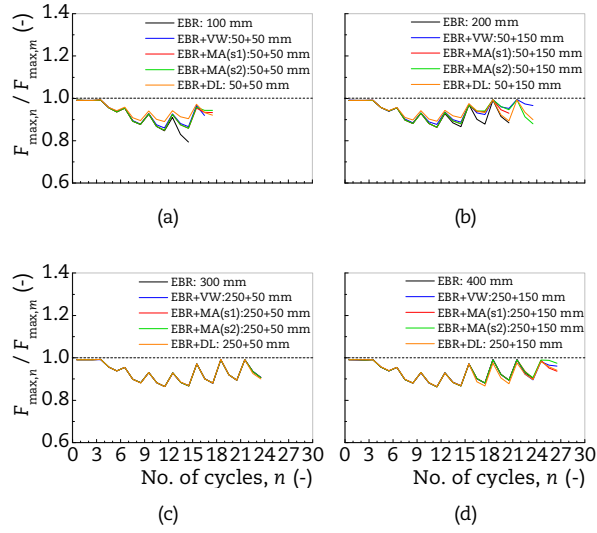


Fig. 6.  $F_{max,n}/F_{max,m}$  of numerical specimens with a total bonded length of (a) 100 mm; (b) 200 mm; (c) 300 mm; and (d) 400 mm.

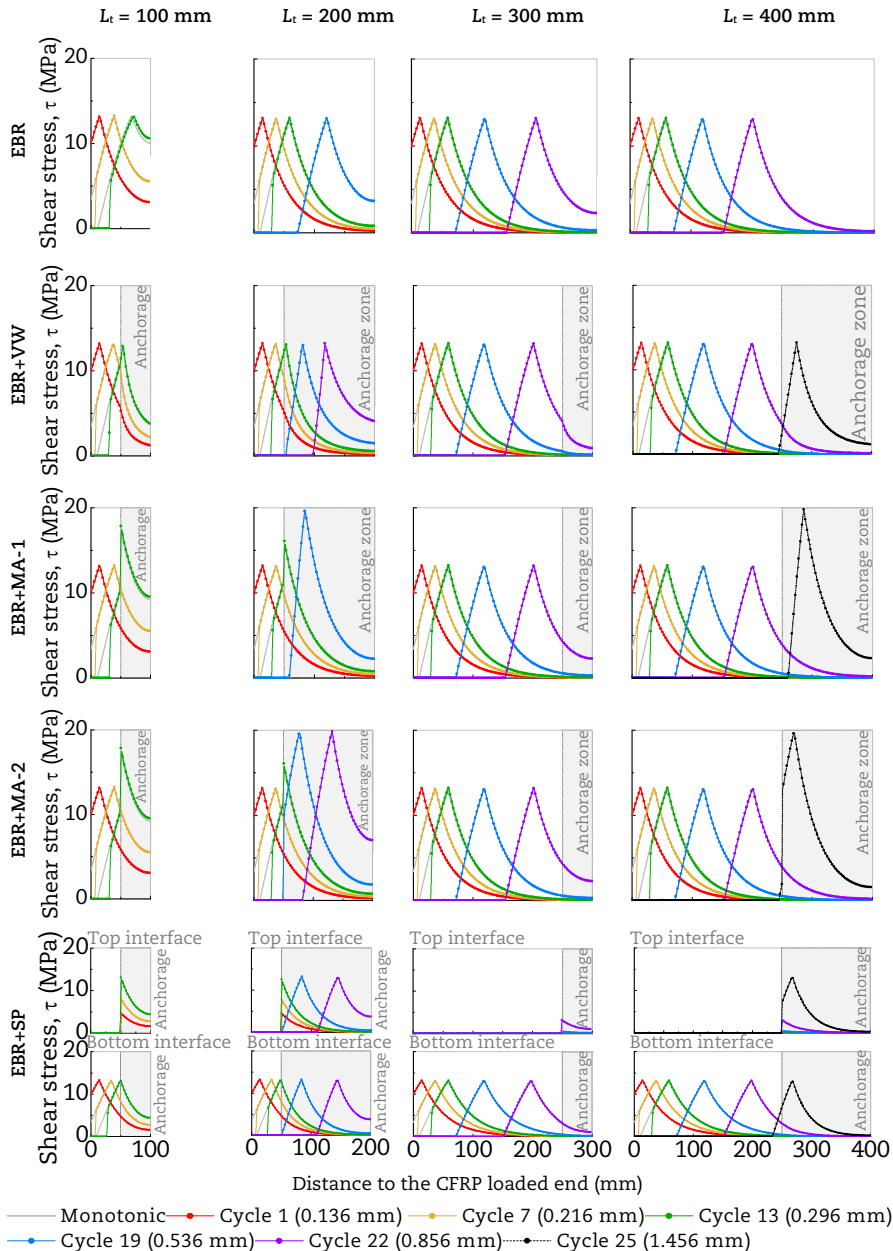


Fig. 7. Shear (or bond) stress distribution of all numerical specimens.



However, it can be seen from Fig. 7 that the damage of the CFRP-to-steel joint firstly occurs in the specimens subjected to the cyclic loading rather than the monotonic loading. For all the CFRP-to-steel bonded joints, at the nominated slip values of 0.216 mm and 0.296 mm, the shear stress values are null near the CFRP loaded end with the cyclic loading. This means that the CFRP strip has already separated from the substrate. On the contrary, with the monotonic loading condition and at the same nominated slips, the shear stress values have not reached a zero value yet or the debonded length is very small if no shear stresses develop at the CFRP pulled end. In the modelling approach used, local interfacial damage occurs during loading and unloading paths when the maximum bond stress value is reached. In these situations, the repetition of the same loading cycles, i.e. at the same interfacial slip, induced a damage progression into the joint which leads to a faster separation of the CFRP laminate from the steel substrate than that observed from the bonded joint under the monotonic loading.

The effect of the type and length of the anchorage on the CFRP strains can be seen in Fig. 8. Either with monotonic and cyclic loading protocols, the failure mode in all modelled anchored joints occurred within the interface as already mentioned. Consequently, the rupture strain of the CFRP was never reached. In fact, the maximum strains developed in the CFRP strips were quite lower than 1.03% which means that the mechanical properties of the CFRP laminate were not fully exploited. The maximum registered CFRP strain value at the pulled end was 0.77% in the EBR+VW specimens with an anchorage length of 150 mm (with  $L_t = 200$  mm and  $L_a = 400$  mm). As the load capacity or strain in the CFRP increases, the more efficient the adopted anchorage is to preserve the integrity of the bonded joint. However, for the same nominated slip at the CFRP pulled end, the CFRP strain (and load) varies with the adopted anchorage system and bonded lengths in both regions, unanchored and anchored. Hence, at the nominated slip of 0.536 mm, the highest CFRP strain values occurred in the anchored bonded joints with a total length of 200 mm (i.e. with  $L_b = 50$  mm and  $L_a = 150$  mm). The short regular bonded region may justify this pattern since at the nominated slip the influence of the mechanical anchorage is revealed sooner. So, the contribution of the mechanical anchorage is carried out by extending the shear stresses throughout the anchorage length and, therefore, resulting in higher loads transmitted to the CFRP strip and increasing the CFRP strain values. On the contrary, when the regular bonded length is longer and assuming the same nominated slip at the CFRP pulled end, the strains developed in the CFRP strip are lower but the debonded length is significantly larger than in the specimens with a regular bond length of 50 mm only (see Fig. 8).

It is also worthy to mention that the CFRP strain distributions along the bonded length are quite similar whether the monotonic or the cyclic loading are applied to the CFRP-to-steel joints. The only differences observed from the curves shown in Fig. 8 can be found for the nominated slips of 0.216 mm and 0.296 mm where the CFRP strain values resulting from the cyclic loading are lower than of the monotonic loading in the vicinity of the CFRP pulled end. This occurs because the load required to reach the nominated slip value is lower (see Fig. 6) and the CFRP has already debonded from the substrate along a small length not exceeding approximately 30 mm.

#### 4.2.3 Analysis of the damage

To assess the damage progression in the CFRP-to-steel bonded joints, Fig. 9 shows the local damage ( $D_n^U$ ) distribution along the bonded length obtained from all specimens subjected either by the monotonic and cyclic loading. To facilitate the comparisons with the specimens monotonically loaded, the same nominated slip points used in subsection 4.2.2 are herein adopted. On the other hand, Fig. 10 shows the global damage parameter ( $L_{d,n}$ ) evolution calculated from all specimens subjected to the loading cycles. It is worth mentioning that for both damage variables, local and global, the absence of damage corresponds to 0 and full damage to 1. Global damage indicates the proportion of the CFRP length that has physically separated from the steel substrate, which development is directly provided by the proposed local bond-slip relationship, i.e. the local contact fails when the accumulated plastic displacement reaches its maximum value which corresponds to the softening branch amplitude.

For the two lowest nominated slip values (0.136 mm and 0.216 mm), since the anchorage zone has been not damaged, the local damage distribution along the bonded length is the same in all specimens, even for the 100 mm-length bonded joints. Thereafter, the damage progression is slower in the anchored specimens, however, this effect can only be seen if the damage enters into the anchorage region. The segment of each curve that  $D_n^U$  varies from 0 to 1 is mostly parallel to other curves obtained at different nominated slip values. However, in some curves such as those with 0.296 mm of the specimens EBR+VW, EBR+MA-1, and EBR+MA-2 with 100 mm-length, this segment comprises several distinct zones when the damage approaches the anchorage zone, which is reflected by a steeper slope. This trend occurs because although the regular bonded length is in the softening stage the anchorage length remains in the elastic stage in which no damage is allowed. In addition, the damage evolution inside the anchorage is carried out more rapidly, i.e. it goes from 0 to 1 with a higher slope (smaller length), in the EBR+VW and EBR+MA-1 (see both graphs with  $L_t = 200$  m) than in the other specimens. In the case of the EBR+VW specimens, although the interface between the CFRP composite and the steel substrate has been modelled through the CZM 1, the width variation has increased the local forces transmitted through the interface and with that a steeper transition of damage along the anchorage length is obtained. On the other hand, the CZM 2, with the most abrupt softening decay (see Fig. 2), was used to model the interface between the CFRP and the steel substrate of EBR+MA-1 specimens. Therefore, and since the definition of the damage depends on the softening stage of the CZM (see Eq. (7)), the damage transition is carried out in a faster way, i.e. the slope shown in the EBR+MA-1 specimen with  $L_t = 200$  mm is higher than in any of the other EBR+MA-2 and EBR+SP specimens.

Similar to the pattern of the distribution of interfacial shear stresses and CFRP strains, the differences in the local damage distribution between the monotonic and cyclic loadings are detected only in the curves corresponding to the nominated slips of 0.216 mm and 0.296 mm. Thereafter, the monotonic and cyclic curves are identical. It is noteworthy to mention that if the curves for the 2<sup>nd</sup> and 3<sup>rd</sup> cycles of each nominated slip value were plotted, the monotonic and cyclic curves would not match because by repeating the cyclic loading at the same nominated slip, it causes the damage progression and, consequently, reduces the transmitted load to the CFRP strip as can be seen from Fig. 6.

Looking now at Fig. 10 with more detail, it can be observed that the debonding trend of the joints under cyclic loading varies with the total bonded length and with the mechanical anchorage. However, it should be kept in mind that the curves shown in Fig. 10 were obtained from a specific loading cycle protocol adopted in this work. The results show that the addition of an anchorage system to a CFRP bonded joint is especially important when the regular bonded length is short. Under such cases, the debonding process is slower, allowing the joint to sustain a higher number of loading cycles. Differently, the beneficial effect of the anchorage system varies from insignificant to fair when the regular bonded length is long. For the total bonded length of 300 mm (i.e. with  $L_b = 250$  mm and  $L_a = 50$  mm), none of the modelled anchorage systems were able to increase the number of loading cycles in comparison with the specimens bonded according to the conventional EBR system. Thus, by increasing the anchorage length from 50 mm to 150 mm that follows the regular length of 250 mm, the number of loading cycles sustained by anchorage joints is increased from 25 to 28 cycles, regardless of the anchorage type system.



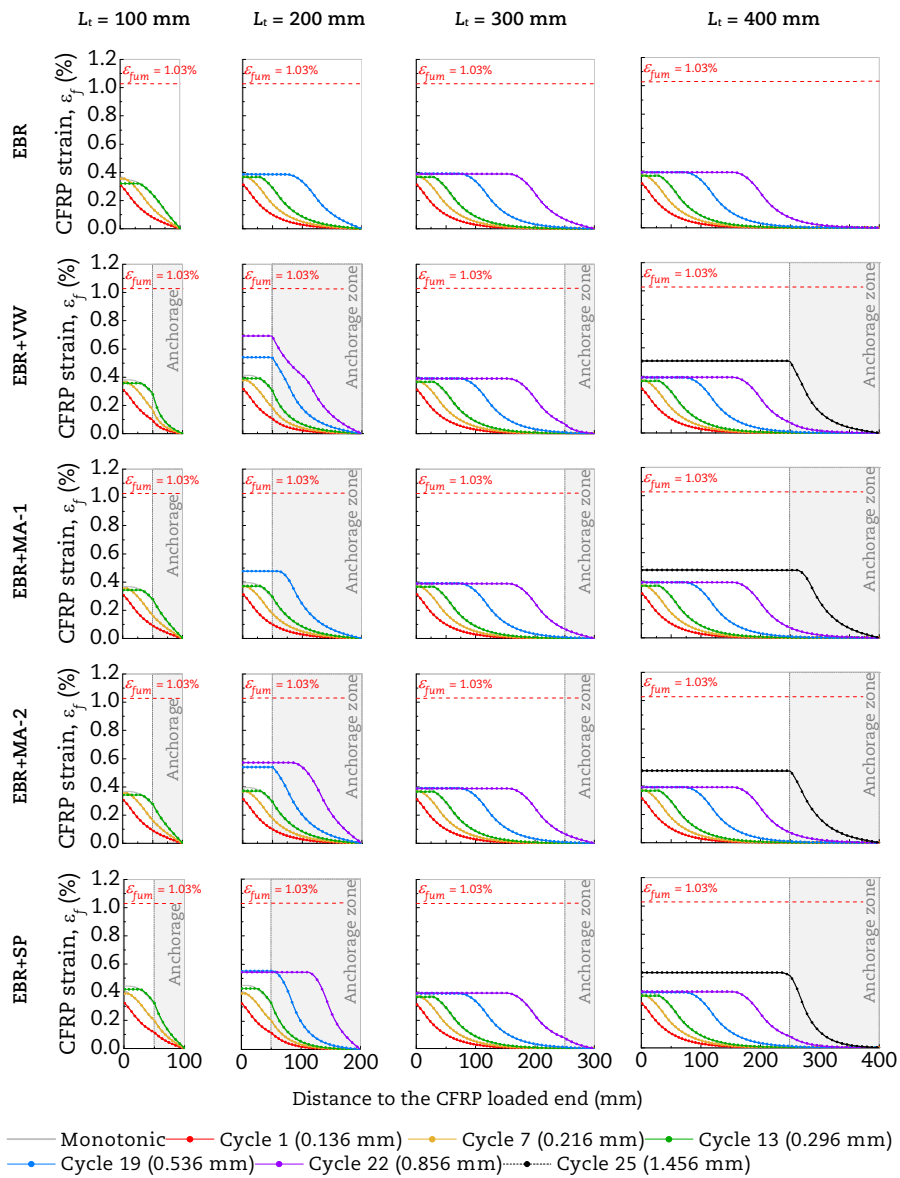


Fig. 8. CFRP normal strain distribution developed in all the numerical specimens.

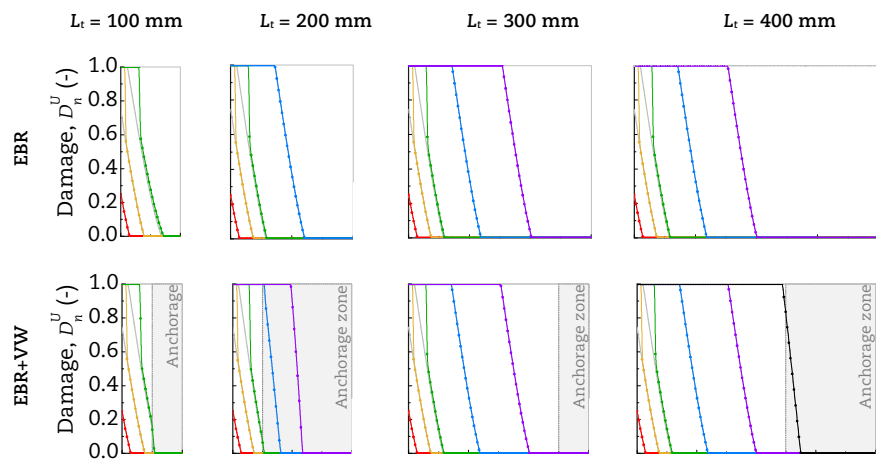


Fig. 9. Local damage condition developed in all the numerical specimens.



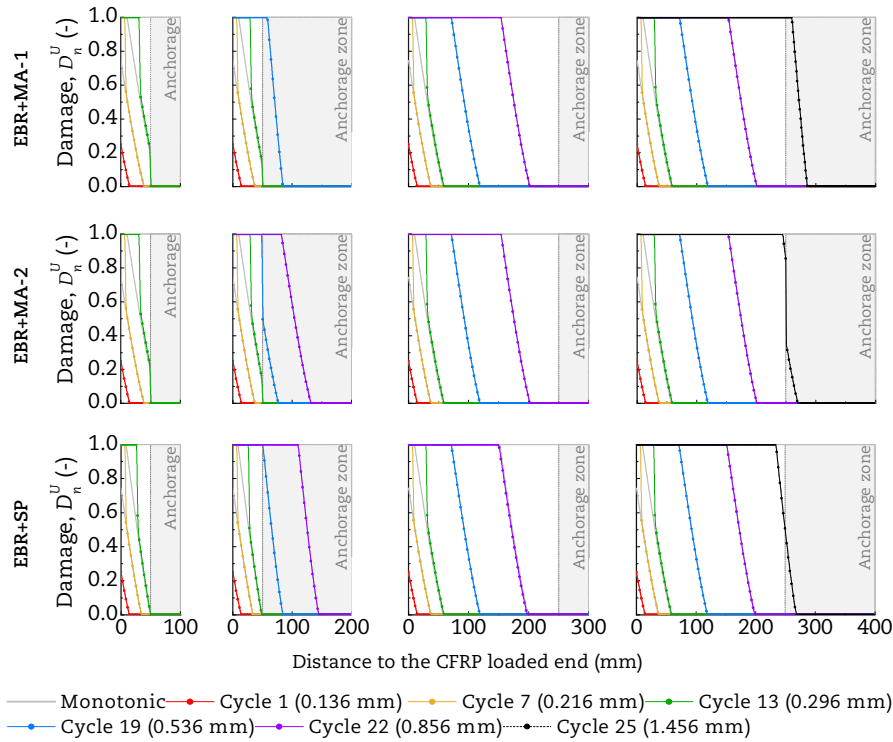
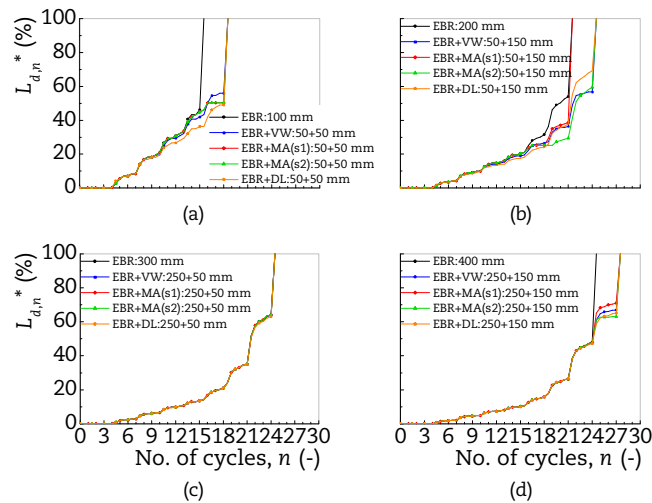


Fig. 9. Continued.


 Fig. 10. Evolution of  $L_{d,n}^*$  with loading cycles for numerical specimens with a total bonded length of: (a) 100 mm; (b) 200 mm; (c) 300 mm; and (d) 400 mm.

#### 4.2.4 Equivalent damping factor

Finally, to assess the performance of the anchored bonded joints to cyclic loading, the viscous damping properties are calculated. It is broadly acknowledged in structural engineering that the structures should have the ability to dissipate part of the input energy from a cyclic loading by damping, thus contributing to accommodate deformation and damage without a considerable reduction in global strength [64]. Often, the dissipation of energy upon repeated loading is identified by a hysteresis loop in the load-deformation curves for each cycle, being quantified by the loop area ( $E_{d,n}$ ). Thus, the hysteresis loop is used to calculate the hysteretic or viscous equivalent damping factor that is responsible for most of the damping in common structural elements. For simple harmonic loading, with complete load-deformation reversal, the equivalent viscous damping factor, in cycle  $n$ , is [65]:

$$\zeta_n = \frac{E_{d,n}}{4\pi E_{s0}} \quad (8)$$

where  $E_{s0}$  is the elastic strain energy, determined as:

$$E_{s0} = \frac{F_{\max} \cdot u_{\max}}{2} \quad (9)$$



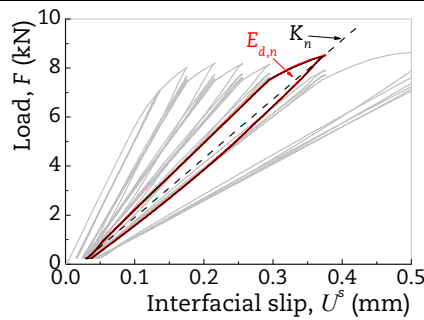


Fig. 11. Calculation of the equivalent damping factor in cycle n.

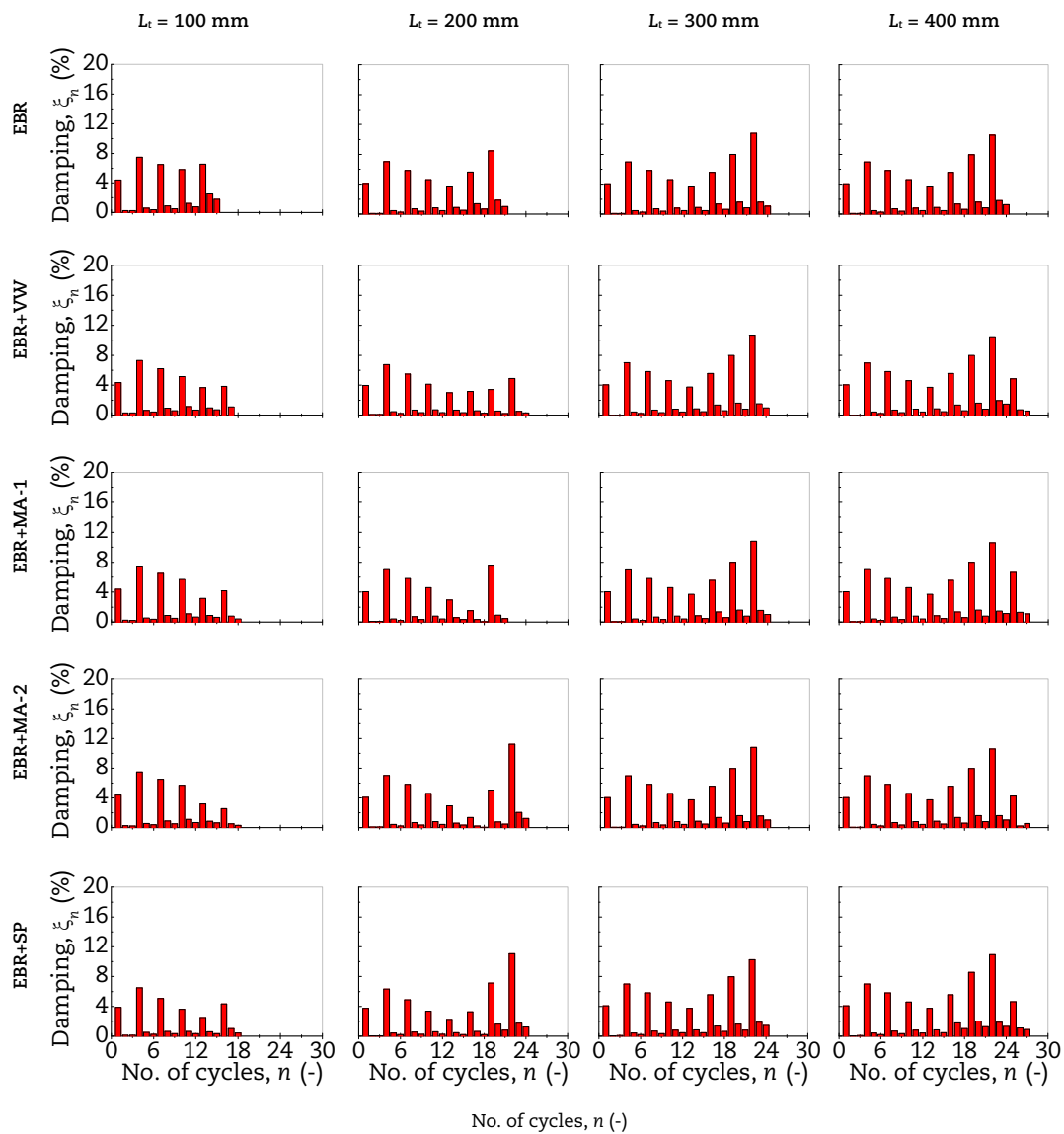


Fig. 12. Calculation of the equivalent damping factor in cycle n.

and  $F_{max}$  and  $u_{max}$  are the maximum load and displacement, respectively. Adapting this formulation to the simulated cyclic loading protocol, illustrated in Fig. 11, the equivalent damping factor in cycle n is determined as:

$$\xi_n = \frac{2E_{d,n}}{\pi K_n \cdot U_{max}^s} \tag{10}$$

where  $K_n$  is average global stiffness and  $U_{max}^s$  is the maximum interfacial slip value.

The results obtained for all specimens subjected to the cyclic loading are plotted in Fig. 12. It can be noticed that the first cycle at the same nominated slip led to the highest equivalent damping ratios whilst the 2<sup>nd</sup> and 3<sup>rd</sup> cycles had lower values (< 2%). This means that the dissipated energy during the first cycle is quite meaningful when compared to the two following cycles. The trend of the equivalent damping ratio corresponding to the first cycles of each nominated slip is similar in all specimens. In other words, the equivalent damping ratio tends to decrease with the number of cycles but when the debonding of the CFRP from the steel substrate has already initiated, the equivalent damping ratio inverts its trend and begins to increase with the number of



cycles. This is explained, once again, by the dissipated energy obtained of the first cycle during the separation of the CFRP from the substrate, which is higher than that obtained during a prior debonding stage where the separation of the CFRP from the steel substrate has not initiated (see Fig. 5).

Considering the specimens with the highest regular bonded lengths (with  $L_b = 250$  mm and  $L_t = 300$  mm or  $L_t = 400$  mm), the equivalent damping ratio has almost not changed from the reference EBR specimens. In these cases, the equivalent damping at the 22<sup>nd</sup> cycle stayed within an interval between 10% and 12%. These results suggest that the mechanical anchorage type or its length are two non sensitive parameters to the equivalent damping ratio once a long relative bonded length is used. However, if the relative bonded length is short, the equivalent damping ratio evolution is sensible to the anchorage type. For the  $L_t = 200$  mm and  $L_a = 50$  mm, the highest equivalent damping ratio was also reached at the 22<sup>nd</sup> cycle for the EBR+MA-2 and EBR+SP specimens, and very similar (11%) to the values obtained for longer bonded lengths. Differently, the other joints resulted in significantly lower damping values.

An overall overview of the calculated equivalent damping ratios allows us to state that these values are not very high, even for the first cycle at any nominated slip value. It should be bear in mind that the present CFRP-to-steel bonded joints have been subjected to a pull-push test, at a single displacement speed, inducing damage in one direction only and with no load reversal. Consequently, and analogous to the work developed by Rodrigues et al. [64] who studied the equivalent damping ratio of columns under axial and biaxial horizontal cyclic loading, the dissipated energy during the loading cycles is expected to be lower than if the bonded joints would be subjected to a mixed mode (II + III), i.e. under a biaxial loading cycle.

## 5. Conclusions

The cyclic bond behaviour of several bonded joints where the CFRP strip was bonded onto the steel substrate through four main different bonding techniques was idealized, numerically simulated, and fully investigated in this study. Based on the collected data herein reported, the subsequent conclusions can be enumerated:

- Whether the bonding technique is used, the CFRP composite has always debonded from the steel substrate. Therefore, the failure mode was always associated with a cohesive rupture within the adhesive rather than cohesive in the CFRP. In this regard, the maximum load transmitted to the CFRP was 15.7 kN (in the EBR+VW specimen with a total length of 200 mm and 400 mm) which is about 31.5% lower than its failure load value of 22.9 kN;
- When the anchorage length is short, the use of a steel plate to anchor the CFRP onto the steel substrate reveals to be the most efficient anchorage. The use of any of the other anchorage systems was not able to improve the final strength of the CFRP-to-steel joints;
- Under the adopted cyclic event, the results reveal that once the regular or the anchorage lengths are sufficiently long, the final strength of CFRP-to-steel bonded joint is not degraded. By imposing a displacement loading control, a reduction of the stiffness and load transmitted to the CFRP was observed in the CFRP-to-steel. However, unlike the forces transmitted to the CFRP composite that can reach the same value obtained from the monotonic test in the latter cycles, the stiffness of the joint tended to continuously degrade with no possible recovering;
- Compared with the monotonic shear (or bond) stress and CFRP strain configurations, the homologous cyclic configurations had not changed significantly. However, the results showed that shear stresses at the CFRP loaded end tended to rapidly decay to a zero value due to the damage progression imposed by the cyclic loading protocol. So, the physical separation of the CFRP strip from the steel substrate occurred at a sooner moment of the CFRP-to-steel debonding process. This phenomenon was visible at the first cycle of each nominated slip value and until the 13<sup>th</sup> cycle. Afterwards, no further differences between the monotonic and cyclic shear stress configuration were observed. Despite not being shown here, it should be mentioned that shear stress configurations of the second and third cycles of each nominated slip value showed some differences from their homologous monotonic configurations, which can be explained by the damage progression generated by the cyclic loading;
- From a global evaluation of the damage developed in the bonded joint, the results showed that the global damage  $L_{d,n}$  is mostly influenced by the regular bonded length. So, in the case of the specimens with a regular length of 250 mm, the differences of the calculated global damages between specimens are insignificant. On the other hand, regarding the local damage  $D_n^U$ , the damage distributions through the total length of the joint follow the same trend of the shear stress configurations;
- The calculated equivalent damping of the specimens always registered higher values at the first cycle of each nominated slip value. In the following second and third cycles, the equivalent damping parameter decreased significantly. This is explained by the amount of dissipated energy during the first cycle which is closely related to the damage developed in the CFRP-to-steel joints.

## Author Contributions

Rui Micaelo suggested the numerical programme, developed the numerical modelling, examined the theory validation and wrote the first draft of the paper; Marta Carvalho analysed the numerical results and wrote the final version of the paper; Raquel Almeida analysed the numerical results and wrote the final version of the paper; Wan-Yang Gao helped on the analyses of the results, examined the theory validation, and wrote the final version of the paper; Hugo Biscaia planned the scheme, initiated the project, suggested the numerical programme, wrote the final version of the paper and supervised the work. The manuscript was written through the contribution of all authors. All authors discussed the results, reviewed, and approved the final version of the manuscript.

## Acknowledgments

The authors gratefully acknowledge the Portuguese Foundation for Science and Technology (FCT - MCTES) for its financial support via the project UIDB/00667/2020 (UNIDEMI).

## Conflict of Interest

The authors declared no potential conflicts of interest concerning the research, authorship, and publication of this article.



## Funding

The authors received financial support from the Portuguese Foundation for Science and Technology (FCT - MCTES) for the research, authorship, and publication of this article.

## Data Availability Statements

The datasets generated and/or analyzed during the current study are available from the corresponding author on reasonable request.

## Nomenclature

$b_f$	The width of bonded layer [mm]	$L_{d,n}^*$	The normalized debonded length of bonded joint [-]
$b_{vw}$	The maximum width of anchorage where the width is linearly increased (VW) [mm]	$F_{max,n}$	The maximum load in monotonic pull-push test [kN]
$D_n^U$	Local damage of interface [-]	$L_a$	The regular bonded length [mm]
$E_{fm}$	Average elastic modulus of CFRP composite [GPa]	$L_b$	The anchorage length [mm]
$E_{d,n}$	Dissipation energy in cycle $n$ [kN.mm]	$L_t$	The total bonded length [mm]
$E_{so}$	Elastic strain energy [kN/mm]	$t_f$	The thickness of bonded layer [mm]
$F$	The load in pull-push test [kN]	$U_{max}^s$	The slip at $\tau_{max}$ of CZM [mm]
$F_{max,n}$	The maximum load in cyclic pull-push test in cycle $n$ [kN]	$U^{n_{ult}}$	The softening branch stiffness of CZM [kN/mm]
$k_d^s$	The accumulated plastic shear displacement of contact in cycle $n$ [mm]	$U_{p,n}^s$	The normal displacement at failure of contact [mm]
$k_e^n$	The elastic slope of CZM [kN/mm]	$U^s$	The interfacial slip at the interface [mm]
$K_n$	The average global stiffness in cyclic pull-push test in cycle $n$ [kN/mm]	$\sigma_{fum}$	The average failure stress of the CFRP composite [MPa]
$L_{d,n}$	The debonded length of bonded joint [mm]	$\epsilon_{fum}$	The strain of the CFRP composite [%]
		$\tau_{max}$	The average failure strain of the CFRP composite [%]
		$\tau_{max,n}$	The maximum bond stress of CZM [MPa]
		$\xi_n$	The stress threshold value of contact in cycle $n$ [MPa]
			The equivalent viscous damping factor in cycle $n$ [-]


## References


- [1] da Silva L.F.M., Adams R.D., Techniques to reduce the peel stresses in adhesive joints with composites, *International Journal of Adhesion and Adhesives*, 27(3), 2007, 227-235.
- [2] Banea M.D., da Silva L.F.M., The effect of temperature on the mechanical properties of adhesives for the automotive industry, *Proceedings of the Institution of Mechanical Engineers, Part L: Journal of Materials: Design and Applications*, 224(2), 2010, 51-62.
- [3] da Silva L.F.M., *Design rules and methods to improve joint strength*. Handbook of Adhesion Technology. Springer, Berlin, Heidelberg, 2011.
- [4] Wu X.F., Zhao Y., Stress-function variational method for interfacial stress analysis of adhesively bonded joints, *International Journal of Solids and Structures*, 50(25-26), 2013, 4305-4319.
- [5] Banea M.D., da Silva L.F.M., Adhesively bonded joints in composite materials: An overview, *Proceedings of the Institution of Mechanical Engineers, Part L: Journal of Materials: Design and Applications*, 223(1), 2016, 1-18.
- [6] SatyanarayanaGupta M., Veeranjanyulu K., Fabrication and analysis of adhesive joints used in aircraft structures, *Materials Today: Proceedings*, 4, 2017, 8279-8286.
- [7] Ayatollahi M.R., Samari M., Razavi S.M.J., da Silva L.F.M., Fatigue performance of adhesively bonded single lap joints with non-flat sinusoid interfaces, *Fatigue Fracture Engineering Materials Structures*, 40(9), 2017, 1355-1363.
- [8] Jeevi G., Nayak S.K., Kader M.A., Review on adhesive joints and their application in hybrid composite structures, *Journal of Adhesion Science and Technology*, 33(14), 2019, 1497-1520.
- [9] Lee D.W., Song J.I., Research on simple joint method using fiber-metal laminate design for improved mechanical properties of CFRP assembly structure, *Composites Part B: Engineering*, 164, 2019, 358-367.
- [10] Yuan H., Teng J.G., Seracino R., Wu Z.S., Yao J., Full-range behavior of FRP-to-concrete bonded joints, *Engineering Structures*, 26(5), 2004, 553-565.
- [11] Liu M., Dawood M., A closed-form solution of the interfacial stresses and strains in steel beams strengthened with externally bonded plates using ductile adhesives, *Engineering Structures*, 154, 2018, 66-77.
- [12] Li Q., Fu M., Xie B., Analyzing the bond behavior of Fiber-Reinforced Polymer (FRP) bars embedded in Engineered Cementitious Composites (ECCs) with the nonlocal continuum rod model, *Mathematical Problems in Engineering*, 2020, 2020, 1710364.
- [13] Martinelli E., Closed-form solution procedure for simulating debonding in FRP strips glued to a generic substrate material, *Fibers*, 9(4), 2021, 22.
- [14] Pan J., Xu Z., Leung C.K.Y., Li Z., Analytical and numerical modelling of FRP debonding from concrete substrate under pure shearing, *Journal of Wuhan University of Technology*, 27, 2012, 142-148.
- [15] Campilho R.D.S.G., Banea M.D., Neto J.A.B.P., da Silva L.F.M., Modelling adhesive joints with cohesive zone models: effect of the cohesive law shape of the adhesive layer, *International Journal of Adhesion and Adhesives*, 44, 2013, 48-56.
- [16] Lin J.P., Wu Y.F., Numerical analysis of interfacial bond behavior of externally bonded FRP-to-concrete joints, *Journal of Composites for Construction*, 20(5), 2016, 04016028.
- [17] Bocciarelli M., A new cohesive law for the simulation of crack propagation under cyclic loading. Application to steel- and concrete-FRP bonded interface, *Theoretical and Applied Fracture Mechanics*, 114, 2021, 102992.
- [18] Zhang H., Zhang L., Liu Z., Qi S., Zhu Y., Zhu P., Numerical analysis of hybrid (bonded/bolted) FRP composite joints: A review, *Composite Structures*, 262, 2021, 113606.
- [19] Nakaba K., Kanakubo T., Furuta T., Yoshizawa H., Bond behavior between fiber-reinforced polymer laminates and concrete, *ACI Structural*, 98(3), 2001, 359-367.
- [20] Yuan H., Teng J.G., Seracino R., Wu Z.S., Yao J., Full-range behaviour of FRP-to-concrete bonded joints, *Engineering Structures*, 26, 2004, 553-565.
- [21] Mazzotti C., Savoia M., Ferracuti B., An experimental study on delamination of FRP plates bonded to concrete, *Construction and Building Materials*, 22(7), 2008, 1409-1421.
- [22] Cornetti P., Carpinteri A., Modelling the FRP-concrete delamination by means of an exponential softening law, *Engineering Structures*, 33(6), 2011, 1988-2001.
- [23] Carrara P., Ferretti D., Freddi F., Rosati G., Shear tests of carbon fiber plates bonded to concrete with control of snap-back, *Engineering Fracture Mechanics*, 78, 2011, 2663-2678.
- [24] Biscaia H.C., Chastre C., Viegas A., A new discrete method to model FRP to-parent material bonded joints, *Composite Structures*, 121, 2015, 280-295.
- [25] Klamer E.L., *Influence of temperature on concrete beams strengthened in flexure with CFRP*, Ph.D. Thesis, Eindhoven University, Netherland, 2009.
- [26] Leone M., Matthys S., Aiello M.A., Effect of elevated service temperature on bond between FRP systems and concrete, *Composites: Part B*, 40, 2009, 85-93.
- [27] Dai J.G., Gao W.Y., Teng J.G., Bond-slip model for FRP laminates externally bonded to concrete at elevated temperature, *Journal of Composites for Construction*, 17(2), 2013, 217-228.





- [28] Biscaia H., Chastre C., Viegas A., Franco N., Numerical modelling of the effects of elevated service temperatures on the debonding process of FRP-to-concrete bonded joints, *Composites Part B: Engineering*, 70, 2015, 64-79.
- [29] Biscaia H., Ribeiro P., A temperature-dependent bond-slip model for CFRP-to-steel joints, *Composite Structures*, 217, 2019, 186-205.
- [30] Silva M.A.G., Biscaia H., Chastre C., Influence of temperature cycles on bond between GFRP and concrete, *ACI Structural Journal*, 110(6), 2013, 977-987.
- [31] Shrestha J., Ueda T., Zhang D., Durability of FRP concrete bonds and its constituent properties under the influence of moisture conditions, *Journal of Materials in Civil Engineering*, 27(2), 2015, A4014009.
- [32] Gravina R.J., Aydin H., Visintin P., Extraction and analysis of bond-slip characteristics in deteriorated FRP-to-concrete joints using a mechanics-based approach, *Journal of Materials in Civil Engineering*, 29(6), 2017, 04017013.
- [33] Pan Y., Xian G., Li H., Effects of Freeze-Thaw Cycles on the behavior of the bond between CFRP plates and concrete substrates, *Journal of Composites for Construction*, 22(3), 2018, 04018011.
- [34] Liang H., Li S., Lu Y., Yang T., Reliability analysis of bond behaviour of CFRP-concrete interface under wet-dry cycles, *Materials (Basel)*, 11(5), 2018, 741.
- [35] Choi K.K., Meshgin P., Taha M.M.R., Shear creep of epoxy at the concrete-FRP interfaces, *Composites Part B: Engineering*, 38(5-6), 2007, 772-780.
- [36] Mazzotti C., Savoia M., Stress redistribution along the interface between concrete and FRP subject to long-term loading, *Advances in Structural Engineering*, 12, 2009, 5.
- [37] Biscaia H., Chastre C., A simple analytical approach for creep analysis of EB-FRP systems, *Key Engineering Materials*, 774, 2018, 42-47.
- [38] Ko H., Sato Y., Bond stress-slip relationship between FRP sheet and concrete under cyclic load, *Journal of Composites for Construction*, 11(4), 2007, 419-426.
- [39] Mazzotti C., Savoia M., FRP-concrete bond behaviour under cyclic debonding force, *Advances in Structural Engineering*, 12, 2009, 6.
- [40] Carloni C., Subramaniam K.V., Savoia M., Mazzotti C., Experimental determination of FRP-concrete cohesive interface properties under fatigue loading, *Composite Structures*, 94, 2012, 1288-1296.
- [41] Carloni C., Subramaniam K.V., Investigation of sub-critical fatigue crack growth in FRP/concrete cohesive interface using digital image analysis, *Composites Part B: Engineering*, 51, 2013, 35-43.
- [42] Martinelli E., Caggiano A., A unified theoretical model for the monotonic and cyclic response of FRP strips glued to concrete, *Polymers*, 6, 2014, 370-381.
- [43] Carrara P., De Lorenzis L., A coupled damage-plasticity model for the cyclic behavior of shear-loaded interfaces, *Journal of the Mechanics and Physics of Solids*, 85, 2015, 33-53.
- [44] Zhou H., Fernando F., Chen G., Kitipornchai, S., The quasi-static cyclic behaviour of CFRP-to-concrete bonded joints: An experimental study and a damage plasticity model, *Engineering Structures*, 153, 2017, 43-56.
- [45] Biscaia H.C., Chastre C., Borba I.S., Silva C., Cruz D., Experimental evaluation of bonding between CFRP laminates and different structural materials, *Journal of Composites for Construction*, 20(3), 2016, 04015070.
- [46] Fernando D., Yu T., Teng J.G., Behavior of CFRP laminates bonded to a steel substrate using a ductile adhesive, *Journal of Composites for Construction*, 18(2), 2013, 04013040.
- [47] He J., Xian G., Debonding of CFRP-to-steel joints with CFRP delamination, *Composite Structures*, 153, 2016, 12-20.
- [48] Biscaia H., Chastre C., Silva M.A.G., Bond-slip model for FRP-to-concrete bonded joints under external compression. *Composites Part B: Engineering*, 80, 2015, 246-259.
- [49] Yang Y., Silva M.A.G., Biscaia H., Chastre, C. CFRP-to-steel bonded joints subjected to cyclic loading: An experimental study, *Composites Part B: Engineering*, 146, 2018, 28-41.
- [50] Dai J., Ueda T., Sato Y., Development of the nonlinear bond stress-slip model of fiber reinforced plastics sheet-concrete interfaces with a simple method, *Journal of Composites for Construction*, 9(1), 2005, 52-62.
- [51] Liu K., Wu Y.F., Analytical identification of bond-slip relationship of EB-FRP joints, *Composites Part B: Engineering*, 43(4), 2012, 1955-1963.
- [52] Obaidat Y.T., Heyden S., Dahlblom, O., Evaluation of parameters of bond action between FRP and concrete, *Journal of Composites for Construction*, 17(5), 2013, 626-635.
- [53] Yang Y., Biscaia H., Chastre C., Silva, M.A.G., Bond characteristics of CFRP-to-steel joints, *Journal of Constructional Steel Research*, 138, 2017, 401-419.
- [54] Kaluza M., Hulimka J., Methacrylate adhesives to create CFRP laminate-steel joints: Preliminary static and fatigue tests, *Procedia Engineering*, 172, 2017, 489-496.
- [55] Biscaia H., Chastre, C., Design method and verification of steel plate anchorages for FRP-to-concrete bonded interfaces, *Composite Structures*, 192, 2018, 52-66.
- [56] Wang H.T., Wu G., Dai Y.T., He X.Y., Experimental study on bond behavior between CFRP plates and steel substrates using digital image correlation, *Journal of Composites for Construction*, 20(6), 2016, 04016054.
- [57] Biscaia H., Chastre C., Theoretical analysis of fracture in double overlap bonded joints with FRP composites and thin steel plates, *Engineering Fracture Mechanics*, 190, 2018, 435-460.
- [58] Biscaia H.C., Micaelo R., Teixeira J., Chastre C., Numerical analysis of FRP anchorage zones with variable width, *Composites Part B: Engineering*, 67, 2014, 410-426.
- [59] Potyondy D.O., Cundall P.A., A bonded-particle model for rock, *International Journal of Rock Mechanics and Mining Sciences*, 41(8), 2004, 1329-1364.
- [60] Azevedo N.M., Lemos J.V., Almeida J.R., A discrete particle model for reinforced concrete fracture analysis, *Structural Engineering and Mechanics: An International Journal*, 36(3), 2010, 343-361.
- [61] Azevedo N.M., Lemos J.V., A 3D generalized rigid particle contact model for rock fracture, *Engineering Computations*, 30(2), 2013, 277-300.
- [62] Biscaia H., Micaelo R., Teixeira J., Chastre C., Delamination process analysis of FRP-to-parent material bonded joints with and without anchorage systems using the Distinct Element Method, *Composite Structures*, 116, 2014, 104-119.
- [63] Biscaia H., Micaelo R., Chastre C., Cyclic performance of adhesively bonded joints using the Distinct Element Method: Damage and parametric analysis, *Composites Part B: Engineering*, 178, 2019, 107468.
- [64] Rodrigues H., Varum H., Arêde A., Costa A., A comparative analysis of energy dissipation and equivalent viscous damping of RC columns subjected to uniaxial and biaxial loading, *Engineering Structures*, 35, 2012, 149-164.
- [65] Chopra A.K. *Dynamics of structures: Theory and applications to earthquake engineering (Subsection 3.9: Equivalent viscous damping)*, Prentice-Hall Inc., Upper Saddle River, NJ, USA, 2001.


## ORCID iD

Rui Micaelo  <https://orcid.org/0000-0001-9910-1458>

Marta Carvalho  <https://orcid.org/0000-0003-2799-305X>

Raquel Almeida  <https://orcid.org/0000-0002-6828-6231>

Wan-Yang Gao  <https://orcid.org/0000-0002-2187-3615>

Hugo Biscaia  <https://orcid.org/0000-0002-4791-5123>



© 2022 Shahid Chamran University of Ahvaz, Ahvaz, Iran. This article is an open access article distributed under the terms and conditions of the Creative Commons Attribution-NonCommercial 4.0 International (CC BY-NC 4.0 license) (<http://creativecommons.org/licenses/by-nc/4.0/>).





**How to cite this article:** Micaelo R., Carvalho M., Almeida R., Gao W.-Y., Biscaia H. Numerical Analysis on the Bond Performance of Different Anchored Joints under Monotonic and Cyclic Pull-push Loading, *J. Appl. Comput. Mech.*, 8(1), 2021, 388–404. <https://doi.org/10.22055/JACM.2021.38500.3266>

**Publisher's Note** Shahid Chamran University of Ahvaz remains neutral with regard to jurisdictional claims in published maps and institutional affiliations.

